

# Strangelet Searches in High Energy Heavy Ion Collisions

K.N. Barish<sup>a</sup> for the E864 Collaboration<sup>b</sup>

<sup>a</sup> Department of Physics and Astronomy, University of California at Los Angeles, 405 Hilgard Ave, Los Angeles, CA 90095

<sup>b</sup> Ames Lab – Univ Bari – BNL – UCLA – Iowa State – Univ Mass – MIT – Penn State – Purdue – USMA – Vanderbilt – Wayne State – Yale

In this contribution I concentrate on the recent results from experiment E864 at the BNL-AGS. E864's recent analysis have achieved sensitivities of approximately  $3 \times 10^{-8}$  per 10% central interaction for the production of charged strangelets and the first analysis for neutral strangelets is near completion. I put the results in the context of coalescence and quark gluon plasma strangelet production models.

## 1. Introduction

Relativistic heavy ion collisions provide an environment that can produce systems with a large baryon number and strangeness content in a small volume. About 400 baryons interact and more than 20  $s\bar{s}$  pairs are produced in a central Au+Pb event at the AGS.

Strange quark matter (SQM) states are  $A > 1$  hadrons which contain strange quarks and within which the constituent quarks are allowed to move freely. The presence of strange quarks lowers the Fermi energy levels compared to that of ordinary quark matter (QM – which contains only up and down quarks). This may mean that SQM is more stable than QM, despite the addition of the more massive strange quark.

Calculations [1–3] based on QCD and the phenomenological bag model suggest that SQM may be meta-stable or even completely stable for a wide range of bag model parameter values, which are otherwise unconstrained by past experiments on nuclear matter. Excluding shell effects, all of the calculations contain the feature that SQM systems become more stable as the baryon number  $A$  increases.

In this contribution, I concentrate on the search for SQM with  $A < 100$  (often referred to as *strangelets*) conducted by experiment E864 at the BNL-AGS.

## 2. Experimental strangelet searches

The production probability for strangelet formation is likely different for different colliding systems and energies. Collisions with heavier systems likely produce a more probable environment for strangelet production. Collisions at AGS energies ( $\approx 11.6 A \text{ GeV}/c$  for Au beams) are likely more favorable for coalescence production due to more limited expansion of the system. In contrast, QGP production may be more prominent at CERN energies ( $\approx 158 A \text{ GeV}/c$  for Pb beams). However, the strangeness distillation mechanism

(the process by which a QGP may evolve into a strangeness rich system) may be weaker at CERN energies due to the lower baryon density.

The experimental search for strangelets in heavy ion collisions began with experiment E814 at BNL-AGS with Si beams [4] (Si+Au). Subsequently, experiments E858 (Si+Au) [5], E878 (Au+Au) [6], and E886 (Au+Pt) [7] conducted strangelet searches. At the CERN-SPS strangelet searches at higher energies have been conducted by experiment NA52 (using S and Pb beams). None of these experiments have seen evidence for strangelet production.

Because the experiments measure only a limited region of phase space a production model is needed to translate null measurements into production limits. All of the experiments use a similar model in which the rapidity ( $y$ ) and transverse momentum ( $p_t$ ) are taken to be uncorrelated:

$$\frac{d^2 N}{dy dp_t} \propto p_t e^{-\frac{2p_t}{\langle p_t \rangle}} e^{-\frac{(y-y_{cm})^2}{2\sigma_y^2}} \quad (1)$$

where  $\langle p_t \rangle$  is the mean transverse momentum,  $y_{cm} = 1.6$  is the center-of-mass rapidity for 11.6 GeV/c Au+Pb collisions, and  $\sigma_y$  is the standard deviation of the rapidity distribution of the strangelet.

The experimental searches, with the exception of E814 and E864, employ focusing spectrometers. These spectrometers, which consist of quadrupole as well as dipole magnets, have acceptance for a fixed rigidity ( $R = p/Z$ , where  $p$  is momentum and  $Z$  charge). They have very small acceptances but have little background and can sample much beam to achieve high sensitivities. However, the disadvantage is that they are strongly dependent upon the production model assumed. E886 and E878 have maximum rigidity settings of 2 GeV/c and 20 GeV/c respectively. These rigidity limitations mean the experiments do not measure near mid-rapidity for higher mass strangelets (i.e.,  $m > 10$  GeV/c<sup>2</sup>).

By contrast, experiment E864 uses an open geometry spectrometer. E864 has now completed its second round of strangelet searches, and is in the process of analyzing further data. The recent results from E864 now represent the most sensitive search to date for most masses and production models. E864 is also the first experiment with the capability to search for neutral strangelets.

### 3. The E864 Spectrometer

A schematic diagram of the E864 spectrometer is shown in Fig. 1. The open geometry design of the E864 spectrometer translates into a large geometric acceptance and leads to an efficient search. The spectrometer consists of two dipole magnets, three segmented hodoscope planes of scintillation counters (206 vertical slats), two stations of straw tube arrays (4 mm diameter tubes), and a lead/scintillating fiber hadronic calorimeter (754 towers) [9]. The spectrometer is designed to measure particles around center-of-mass rapidity ( $y_{cm} = 1.6$ ) because this is where we expect strangelet production to be peaked. For the strangelet analysis, E864 searches over an approximate rapidity range from  $y = 1.1$  to  $y = 2.1$ .

The charge ( $Z$ ) of a particle that traverses the spectrometer is measured using pulse height information from the 3 hodoscope walls. Its rigidity ( $R$ ) is derived from the target

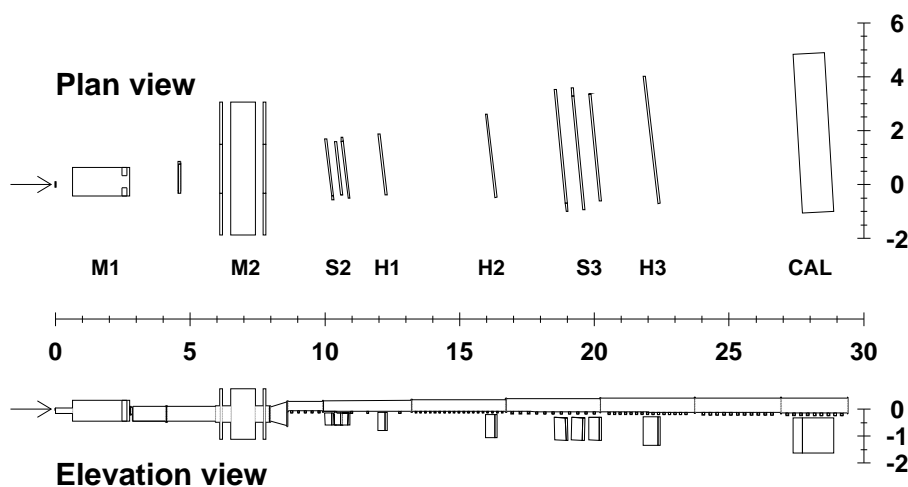


Figure 1. The 1995 configuration of the E864 spectrometer. In the plan view, the downstream vacuum chamber is not shown. M1 and M2 are dipole analyzing magnets, S2, and S3 are straw tube arrays, H1-H3 are scintillator hodoscopes, and CAL is a hadronic calorimeter. The horizontal and vertical scales are in meters.

position and downstream slope and position of the particle's track as measured by the straw tube and hodoscope detectors. The particle's velocity is measured using timing information from the hodoscopes, giving the relativistic quantities  $\beta$  and  $\gamma$ . The particle's mass ( $m$ ) is then reconstructed as  $m = \frac{R}{\gamma\beta}Z$ . The calorimeter's time and energy information is used to confirm above measurements, reject potential backgrounds, and make measurements for neutral particles.

In order to achieve high sensitivities, the detector is able to record 1000-2000 events every 4 seconds (AGS spill). E864 is able to sample several million Au+Pb interactions per second with the implementation of two hardware triggers: a centrality trigger and a high-mass trigger (or Late-Energy Trigger – LET).

The centrality trigger uses a segmented scintillation multiplicity counter which is located 13 cm downstream the target. The multiplicity counter system, which measures the interaction's products within an angular range of  $16.6^\circ$  and  $45^\circ$  with respect to the incident beam direction, provides a rough measure of the impact parameter, or centrality, of the reaction [10]. For this analysis, events with the 10% highest pulse heights, or roughly the 10% most central events are selected.

The calorimeter is used to provide a high-level hardware trigger which selects high-mass objects. The time and energy from each tower are used to make a rough mass measurement ( $m = E/(\gamma - 1)$ ). A programmable lookup table to select high-mass objects is loaded for each tower. With this trigger, an enhancement of  $> 50$  for high-mass objects in the recorded data sample was achieved.

Table 1  
Summary of E864 Recorded Data

Data	Target	Central Events Recorded	LET Enhancement	Sampled Central Collisions
1994 “+1.5T”	10% Pb	$26.5 \times 10^6$	N/A	$2.7 \times 10^7$
1995 “+1.5T”	30% Pb	$27.0 \times 10^6$	55	$1.5 \times 10^9$
1995 “-0.75T”	30% Pb	$85.5 \times 10^6$	55	$4.7 \times 10^9$
1996 “+1.5T”	60% Pt	$185.0 \times 10^6$	73	$13.5 \times 10^9$
1996 “-0.75T”	60% Pt	$217.0 \times 10^6$	77	$16.7 \times 10^9$

## 4. Recorded Data

The E864 spectrometer was commissioned during the Fall 1994 run of the experiment. Only 1/4 of the calorimeter was completed and there was no high-mass trigger. For the 1995 experimental run, the calorimeter and high-mass trigger were fully implemented.

A summary of the data recorded by experiment E864 is shown in Table 1. The “+1.5T” data is optimized for the positive strangelet search, while the “-0.75T” data is optimized for the negative strangelet search. All data was taken with a 11.6 A GeV/c Au beam.

## 5. Results from E864 Strangelet Searches

### 5.1. Charged Strangelet Analysis

From the 1994 analysis [11,12], E864 observed 25  $Z = +1$  strangelet candidates with masses from 10 – 200 GeV/c<sup>2</sup>. However, from GEANT simulations carried out during the design phase of the experiment, a class of  $Z = +1$  backgrounds was expected for the 1994 configuration of the detector from neutrons which undergo inclusive charge exchange reactions ( $n + A \rightarrow p + X$ ) after the second magnet but before the first detector. The protons can travel in a similar direction to the original neutron, which does not bend in the magnetic field. Therefore, the reconstructed tracks resulting from this process appear to have a high rigidity and thus a high mass. E864 performed studies to compare their observations to their expectations that the backgrounds were due to charge exchange and concluded that the high mass candidates are consistent with the expected background. Thus, E864 placed upper limits on strangelet production.

In addition to the tracking system, the full calorimeter is used for the 1995 analysis. Fig. 2 illustrates the power of the calorimeter. Plotted is the mass calculated from the energy deposited in the calorimeter and time at the calorimeter ( $m = E_{dep}/(\gamma - 1)$ ) versus the associated mass reconstructed by the tracking system for the “-0.75T” 1995 data. Cuts have been applied to ensure that the calorimeter energy is not contaminated from other showers, and tracking  $\chi^2$  cuts to fits in the bend plane, vertical plane, and time have been applied to ensure good tracks. The time at the calorimeter is derived from a fit to the hodoscope times because this provides a more accurate time measurement than using the time derived from the calorimeter. Note that the target point is not included in this fit to allow for tracks which do not originate from the target. From this figure, it can be seen that the tracks which reconstruct with a high mass from the tracking detectors

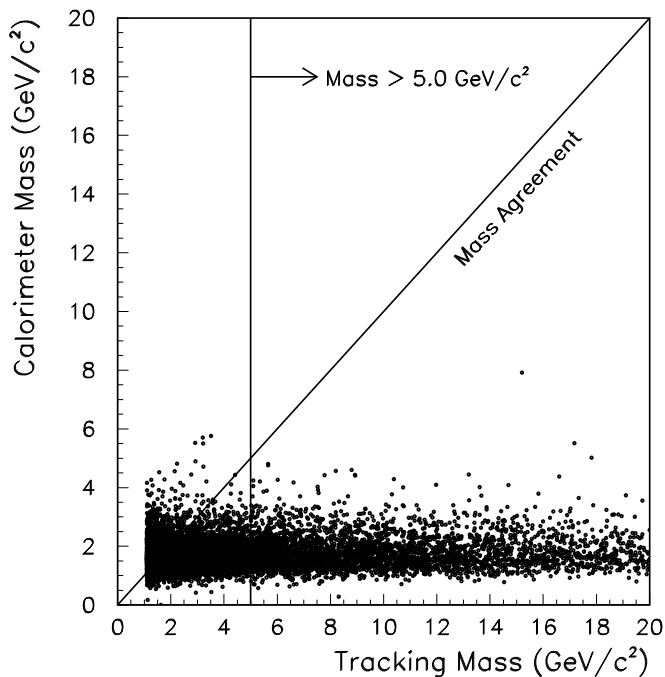


Figure 2. A scatter plot of  $Z = -1$  high-mass candidates' tracking mass versus calorimeter reconstructed mass. The data represents the complete “ $-0.75T$ ” 1995 data sample after calorimeter contamination cuts and track cuts have been applied.

do not have a correspondingly high calorimeter mass. Indeed, when agreement between the calorimeter and tracking chambers is imposed, all of the high-mass candidates are eliminated.

For the “ $+1.5T$ ” positive strangelet search [12,13], no candidates were observed for  $Z = +1$  with  $m > 5 \text{ GeV}/c^2$ , or for  $Z = +2$  with  $m > 6 \text{ GeV}/c^2$ .

For the “ $-0.75T$ ” strangelet search [12,14], no candidates were observed for  $Z = -1, -2$  with  $m > 5 \text{ GeV}/c^2$ . Because of our large geometric acceptance, E864 was also able to search for positive strangelets with this spectrometer setting. These limits are combined with the “ $+1.5T$ ” limits to produce our final sensitivities.

E864 does observe clear peaks in their mass distributions for  $Z = 1$  objects such as  $p$ ,  $d$ ,  $t$ ,  $K^-$ , and  $\bar{p}$ , and  $Z = 2$  objects such as  ${}^3\text{He}$ ,  ${}^4\text{He}$ , and  ${}^6\text{He}$ . For the 1995 data sample E864 sees over 50  ${}^6\text{He}$  nuclei measured within  $\pm 0.6$  units of mid-rapidity.

## 5.2. Neutral Strangelet Analysis

The production of neutral strange quark matter in heavy ion collisions is previously unconstrained by experimental measurements. E864 is able to be sensitive to neutral strangelets with use of the hadronic calorimeter.

The hodoscope and straw tube tracking chambers are used to identify charged particles entering the calorimeter. The calorimeter showers which these correspond to are rejected. The energy and timing information from the calorimeter is then used to reconstruct the mass of neutral particles.

### *E864 Neutral Strangelet Candidates*

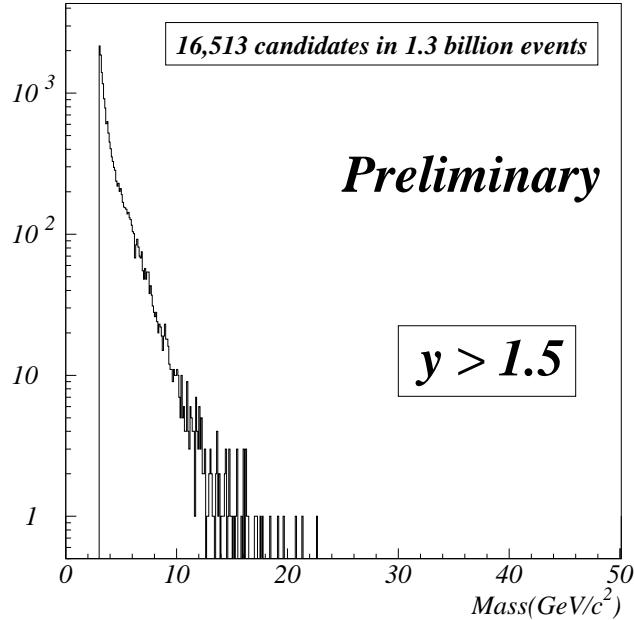


Figure 3. Neutral candidates after charged particle subtraction.

Unlike the charged strangelet analysis, in which the rejection power of the tracking system is utilized, the neutral analysis is expected to be limited by backgrounds. Three source of expected background are overlapping neutron showers, charged particles which have not been identified by the tracking system, and “double interaction” events in which a second interaction occurs after the original interaction and deposits energy in the calorimeter. An example mass distribution from the 1995 “+1.5T” data sample is shown in Fig. 3. [15]. A detailed analysis to optimize the charged particle subtraction and to understand the neutral mass distribution is underway.

E864 will have sensitivity for low mass neutral states, such as the quark alpha state (a single quark bag consisting of 6 up, 6 down, and 6 strange quarks), as well as higher mass states.

### **5.3. Limits on Strangelet Production**

The results from the 1994 and 1995 charged strangelet searches are shown in Fig. 4. The solid lines correspond to  $Z = \pm 1$ , while the dashed lines correspond to  $Z = \pm 2$ .

E864’s upper limits are nearly flat as a function of mass, owing to the large acceptance of the spectrometer. These limits are only mildly sensitive to changes in Eq. 1 for the same reason. For example, if the rapidity width of strangelet production were taken to be  $y = 0.5/\sqrt{A}$ , the E864 curves in Fig. 4 would be lower (give better limits) by less than a factor of 2.

A comparison between the 1994 and 1995 limits show an improvement of well over two orders of magnitude. This is possible because the calorimeter provides additional background rejection, and the high mass trigger allows us to sample more events.

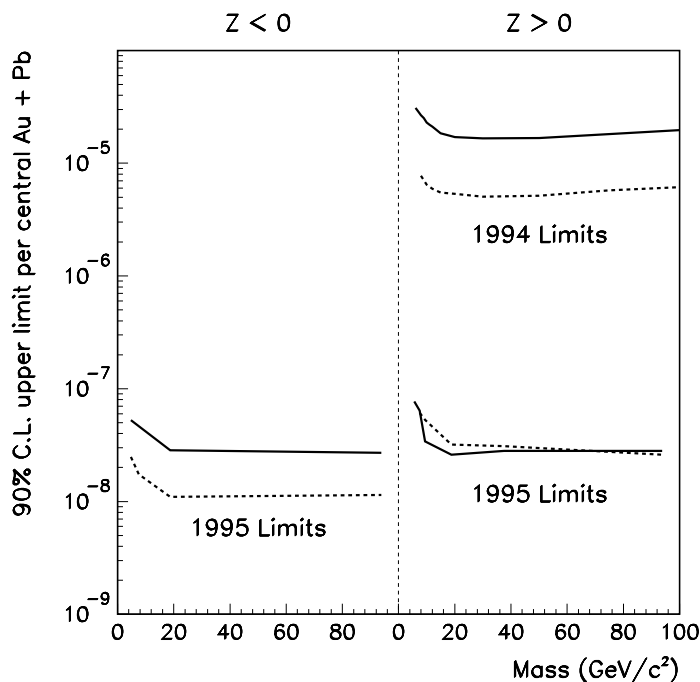


Figure 4. 90% confidence level limits in 10% central collisions for  $Z = \pm 1$  and  $Z = \pm 2$  strangelet production with lifetimes in excess of 40 ns. The solid lines correspond to  $Z = \pm 1$ , while the dashed lines correspond to  $Z = \pm 2$ .

E864 has estimated a preliminary sensitivity for neutral strangelets in the absence of background (e.g.  $m \gtrsim 30$ ) from the 1995 “+1.5T” data. The preliminary sensitivity is approximately  $1 \times 10^{-7}$  per 10% central Au+Pb interaction.

## 6. Interpretation of Strangelet Limits

Ideally, one would like to be able to translate sensitivity limits into constraints on the bag model parameters. However, with the current state of the theories regarding strangelet production and stability this is not possible. But the limits can be compared to the available predictions from coalescence and quark-gluon plasma models.

In order to compare E864’s limits with the predictions of some models, the difference between the measurements in minimum bias and 10% central events must be accounted for. Since strangelet production requires the ingredients of many baryons and many units of strangeness, it is expected that the probability to produce strangelets is greater in central interactions than in peripheral interactions. Ref. [16] predicts that roughly 50% of the production probability for an  $A = 6$  hypernucleus with 2 units of strangeness resides in the 10% most central events. Thus, for comparison we assume that 50% of the strangelet production resides in the top 10% most central collisions by dividing the central limits by a factor of 5.

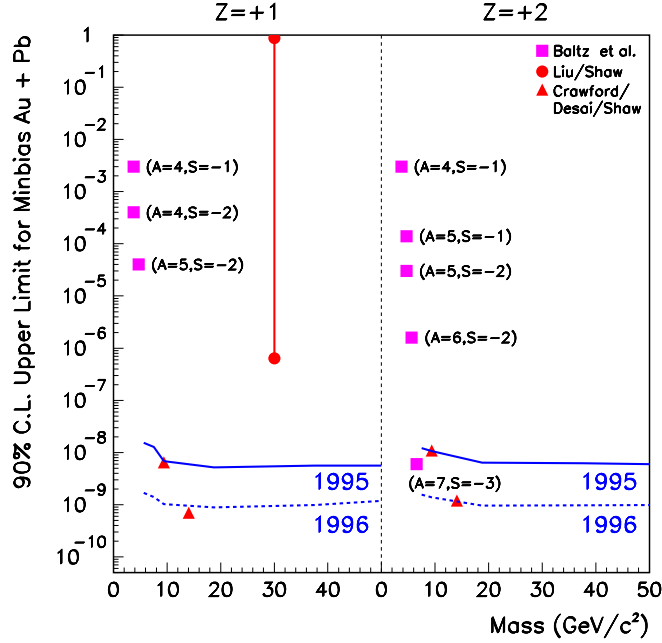


Figure 5. Comparison between E864’s limits and predictions from some models. For the comparison, the limits are divided by a factor of 5 to convert the central limits to minbias (see text). The line labeled 1995 are the limits from the “+1.5T” 1995 run. The dotted lines labeled 1996 are the projected sensitivities from the 1996 run given the amount of data recorded and known LET enhancement. The solid squares are predictions based on the coalescence model from Ref. [16]. The solid circles with the line are the range of predictions based on QGP formation from Ref. [21]. The solid triangles are predictions based on QGP formation from Ref. [20].

### 6.1. Coalescence Models

Heavy ion collisions, in which many hyperons are produced in a small region of phase space, is an environment in which strangelets may be produced by coalescence. In this model, the ingredients of a strangelet (baryon number, strangeness, and charge), in the form of ordinary baryons, can fuse to form a strangelet. Predictions from Ref. [16] are shown in Fig. 5. One might conclude that E864 is beginning to address coalescence predictions for low masses. However, the reader must be cautioned that when taking the predictions from Ref. [16], one can infer that this model over predicts the experimentally observed yields of  $^3\text{He}$  and  $^4\text{He}$  presented in Ref. [17]. Further work is required to interpret the sensitivity in the context of coalescence models.

### 6.2. Quark-Gluon Plasma Models

In another class of models, a strangelet could result from the formation of a quark-gluon plasma (QGP). These production models require (1) that a QGP is produced, and (2) that the QGP charges up with strange quarks compared to non-strange quarks and cools down into a strangelet.



For the first step, Kapusta *et al.* [18] propose that most collisions at AGS energies produce superheated hadronic matter. However, in rare events, a droplet of QGP is nucleated, converting most of the matter to plasma. They calculate the probability that thermal fluctuations in a superheated hadronic gas will produce a plasma droplet, and that this droplet will be large enough to overcome its surface free energy to grow. They estimate the probability for this to occur to be on the order of once every 10 to once every 1000 central collisions. A high mass strangelet would be an experimental signature from which we could infer the formation of a QGP even if it was a rare occurrence. For the second step, Greiner *et al.* [19] suggest that a QGP would likely evolve into a strangelet via the process of strangeness distillation (assuming that strangelets are meta-stable). In this process, once a QGP is formed, it will cool by emitting mesons.  $\bar{s}$  quarks will preferentially find  $u$  and  $d$  quarks to form  $K$  mesons in a baryon rich plasma, such as would be formed at AGS energies. The QGP charges up with strange quarks relative to anti-strange quarks when the mesons are emitted by the plasma. After the system cools down, a strangelet may be formed. These strangelets would likely be massive because the size of the produced QGP could be large, and the large strangelets are postulated to be the most stable.

The data restricts these processes at the 90% confidence level approximately as follows:

$$\text{BR}(\text{Au} + \text{Pb} \rightarrow \text{QGP}) \times \text{BR}(\text{QGP} \rightarrow \text{Strangelet}) < 2.5 \times 10^{-8} \quad (2)$$

where  $\text{BR}(\text{Au}+\text{Pb}\rightarrow\text{QGP})$  is the probability for a central Au+Pb collision at 11.6  $A$  GeV/ $c$  to produce a QGP, and  $\text{BR}(\text{QGP}\rightarrow\text{Strangelet})$  is the probability of the QGP to cool into a strangelet. Equation 2 is approximately valid for strangelets with masses between 10 and 100 GeV/ $c^2$ .

Previously, there have been numerical predictions on the production rate of strangelets assuming QGP formation. Predictions by Crawford *et al.* [20] are the solid triangles in Fig. 5. The original predictions were for Si+Au collisions, but they provided a formula which was applied to derive their Au+Au predictions. E864 is beginning to achieve sensitivities which address their predictions.

Liu and Shaw [21] made the first predictions for strangelet formation. Their predictions are for Si beams, and are quite model dependent. However, one might expect higher production rates with heavier Au+Pb collisions. Their range of predictions, shown in Fig. 5 by a solid line connecting two circles, are ruled out by E864's measurements.

## 7. Prospects for the Future

E864 will finish with the 1995 neutral analysis and continue with the the 1996 neutral and charged analysis. Given the amount of data recorded during the 1996 run, the positive strangelet sensitivity should improve by roughly a factor of 10 (see the dashed line in Fig. 5) and the negative strangelet sensitivity should improve by roughly a factor of 3.5. The 1996 data is also being used to search for strangelets with  $|Z| > 2$ . E864 has already seen  $Z = 3$  objects such as  ${}^6\text{Li}$  from small sample of the 1996 data set. Schaffner *et al.* [22] have recently made calculations indicating that low mass strangelets with large negative charges are more likely to be seen. The sensitivity to neutral strangelets will also improve significantly with the 1996 data. In addition to the increase in data volume,

improvements were made to help suppress the “double interaction” background which was seen in the 1995 analysis.

The current round of strangelet experiments are sensitive only to strangelets with lifetimes in excess of  $\approx 40$  ns. Strangelets are theorized to become more stable as they become more massive. Therefore, it is likely that even if stable strangelets exist, they have masses larger than can be produced via the coalescence mechanism. However, if the lighter strangelets are meta-stable, it would be possible to study them if the experiments were sensitive to particles with lifetimes similar to hyperons. Hopefully experiments will be built which are sensitive to these shorter lived strangelets.

## 8. Acknowledgments

E864 would like to thank the BNL AGS staff for providing the Au beam for the experiment. This work was supported by grants from the U.S. Department of Energy’s High Energy and Nuclear Physics Divisions, the U.S. National Science Foundation, and the Istituto Nazionale di Fisica Nucleare of Italy.

## REFERENCES

1. S.Chin and A.Kerman, Phys. Rev. Lett. **43**, 1292 (1979).
2. E.Farhi and R.Jaffe, Phys. Rev. D **30**, 2379 (1984).
3. E.Gilson and R.Jaffe, Phys. Rev. Lett. **71**, 332 (1993).
4. Experiment E814: J.Barrette *et al.*, Phys. Lett. **B252**, 550 (1990).
5. Experiment E858: A.Aoki *et al.*, Phys. Rev. Lett. **69**, 2345 (1992).
6. Experiment E878: D.Beavis *et al.*, Phys. Rev. Lett. **75** 3078 (1995).
7. Experiment E886: A.Rusek *et al.*, Phys. Rev. C **54**, R15 (1996).
8. Experiment NA52: K.Borer *et al.*, Phys. Rev. Lett. **72**, 1415 (1994).
9. T.A.Armstrong *et al.*, to appear in NIM (1997).
10. P.Haridas *et al.*, NIM A **385**, 412 (1997).
11. K.N.Barish, Ph.D. Thesis, Yale University (1996).
12. Experiment E864: T.A.Armstrong *et al.*, Phys. Rev. Lett. **79**, 3612 (1997).
13. S.Coe, Ph.D. Thesis, Yale University (1997).
14. J.L.Nagle, Ph.D. Thesis, Yale University (1997).
15. M.G.Muhnoz, Ph.D. Thesis in preparation, Wayne State University.
16. A.Baltz *et al.*, Phys.Lett. **B325** 7 (1994).
17. J.K Pope for the E864 Collaboration, in *Proceedings of Heavy Ion Physics at the AGS (HIPAGS)*, Detroit, 1996, edited by C.A. Pruneau *et al.* (Wayne State University report No. WSU-NP-96-16, 1996), p. 119.
18. J.Kapusta *et al.*, Phys. Rev. C **51**, 901 (1995); J.Kapusta and A.Vischer, Phys. Rev. C **52**, 2725 (1995).
19. C.Greiner *et al.*, Phys. Rev. Lett. **58**, 1825 (1987); C.Greiner and H.Stöcker, Phys. Rev. D **44**, 3517 (1991).
20. H.Crawford *et al.*, Phys. Rev. D **45**, 857 (1992).
21. H.C.Liu and G.L.Shaw, Phys. Rev. D **30**, 1137 (1984).
22. J.Schaffner-Bielich *et al.*, Phys. Rev. C **55**, 3038 (1997).